

Short Communication

## Preparation and Property of $\text{Cu}_{50}\text{Zr}_{50-x}\text{Y}_x$ Amorphous Alloy

Xiang Li<sup>1</sup>, Fang Liu<sup>1</sup>, Shuang Wu<sup>1</sup>, Yaoliang Geng<sup>2</sup>, Jie Yang<sup>2</sup>, Yuxin Wang<sup>2,\*</sup>

<sup>1</sup> School of Materials Science and Engineering, University of Shanghai for Science and Technology, Shanghai 200093, China

<sup>2</sup> School of Materials Science and Engineering, Jiangsu University of Science and Technology, Zhenjiang 212003, P. R. China

\*E-mail: [ywan943@163.com](mailto:ywan943@163.com)

Received: 6 January 2017 / Accepted: 17 April 2017 / Published: 12 June 2017

---

Cu-Zr bulk metallic glasses (BMGs) have aroused wide concern recently as they have good glass forming ability, excellent mechanical property, high corrosion resistance and relatively low cost. In this research, different amount of rare earth Y were added in order to improve the glass forming ability of Cu-Zr alloy. The microstructure and glass forming ability of  $\text{Cu}_{50}\text{Zr}_{50-x}\text{Y}_x$  ( $0 \leq x \leq 4\text{at.}\%$ ) alloys were analyzed by using X-ray diffraction (XRD) and differential scanning calorimetry (DSC), respectively. The results show that the addition of Y element can enhance the glass forming ability of Cu-Zr-Y alloys. Meanwhile, the mechanical property of Cu-Zr-Y alloys was significantly improved comparing with that of Cu-Zr alloy. The influence of Y element on the corrosion resistance of Cu-Zr-Y alloys was discussed as well.

---

**Keywords:** Cu-Zr bulk metallic glasses, Glass forming ability, Mechanical property

### 1. INTRODUCTION

Bulk metallic glasses (BMGs) have excellent mechanical properties, good magnetic properties, unique electrical properties and high corrosion resistance [1-3]. In recent years, Copper based metallic glasses were developed as a new type of structural materials [4-6]. Cu-Zr alloys are typical copper based metallic glasses and have been widely studied due to their low cost, high strength and good corrosion resistance. However, due to their limited glass forming ability, further application of Cu-Zr bulk metallic glasses was restricted by their critical size [7-9].

Great efforts were being made to increase the glass forming ability of Cu-Zr alloys. Different elements were added to modify the melting point and glass transition temperature of alloys [10-13].

Inoue et al. (2001) reported that partially substituted Zr by using Ti element can enhance the glass forming ability and increase the critical diameter of Cu-Zr alloy [14]. Wang et al. (2004) found that the addition of Al can improve the thermal stability and glass forming ability of Cu-Zr alloy [15]. Recently, rare elements were utilized to improve the glass forming ability of Cu-Zr alloy. It was convinced that the addition of rare elements can increase the atomic size difference and significantly increase the thermal stability of glass [16]. Our previous research presented that proper addition of Nd element can effectively improve the glass forming ability and mechanical property of Cu-Zr alloys [17]. Zhang et al. (2002) found that the addition of Y element can increase the glass forming ability of Cu-Zr-Ti alloys. Considering the negative heat of mixing between different two elements, it can be predicted that the Y addition should greatly enhance the glass forming ability of Cu-Zr alloys [18].

In this study, rare element Y was added in order to modify the glass forming ability and property of Cu-Zr alloy.  $\text{Cu}_{50}\text{Zr}_{50-x}\text{Y}_x$  ( $0 \leq x \leq 4$ at.%) alloys were prepared by suction casting with copper mold. Their microstructure, glass forming ability, mechanical property and corrosion resistance were systematically investigated.

## 2. EXPERIMENTAL DETAILS

### 2.1 Sample preparation

The master alloy ingots with compositions of  $\text{Cu}_{50}\text{Zr}_{50-x}\text{Y}_x$  ( $x=0, 1, 2, 3, 4$ ) were prepared by arc melting under argon atmosphere. The purities of elements used for sample preparation are 99.999 mass%. The alloy ingots were re-melted for 5 times in order to achieve good element distribution. Amorphous rods with a diameter of 3mm were prepared by copper mold suction casting method. The amorphous cylindrical rods were mechanically polished up to a mirror finish, then degreased ultrasonically in ethanol for characterization.

### 2.2 Sample characterization

The phase structure of alloy rods were characterized by using X-ray diffraction (Bruker D8 Focus X-ray diffractometer, Cu-K $\alpha$  radiation,  $\lambda = 0.15406$  nm). The thermal properties of alloy rods (including glass transition temperature ( $T_g$ ), crystallization temperature ( $T_x$ ) and liquid temperature ( $T_l$ )) were determined by Differential Scanning Calorimetry (DSC) technique under argon gas atmosphere with the flowing rate of 20 mL/min. The DSC curves of samples were obtained under a constant heating rate of 20 K/min. The mechanical property of samples was tested by using Vickers microhardness tester under a load of 100g with a holding time of 15s. Each sample was measured for 10 times in order to eliminate the errors. Corrosion behaviors of Cu-Zr-Y alloys were measured by using an electrochemical workstation (PARSTAT 2273) which equipped with a classical three-electrode system. All the potentiodynamic polarization tests were conducted at room temperature in 0.1mol/L NaCl solution with a scanning rate of 0.33mV/s. The exposed surface area of samples was 1  $\text{cm}^2$ .

### 3. RESULTS AND DISCUSSION

#### 3.1 Microstructure

Fig. 1 presents the XRD patterns of  $\text{Cu}_{50}\text{Zr}_{50-x}\text{Y}_x$  ( $x=0, 1, 2, 3, 4$ ) rod samples.  $\text{Cu}_{50}\text{Zr}_{50}$  alloy has a semi-crystalline structure with a predominant phase of ZrCu. After adding Y element, the structure of rod samples varied significantly.  $\text{Cu}_{50}\text{Zr}_{49}\text{Y}_1$  has a clearer crystalline structure than  $\text{Cu}_{50}\text{Zr}_{50}$  alloy. There is an obviously broad peak around  $2\theta = 38^\circ$  in the diffraction curve of  $\text{Cu}_{50}\text{Zr}_{48}\text{Y}_2$  alloy, indicating that the fabricated rod is fully amorphous. When further increasing the addition of Y element, the peaks which allocated to ZrCu grow sharper and sharper.

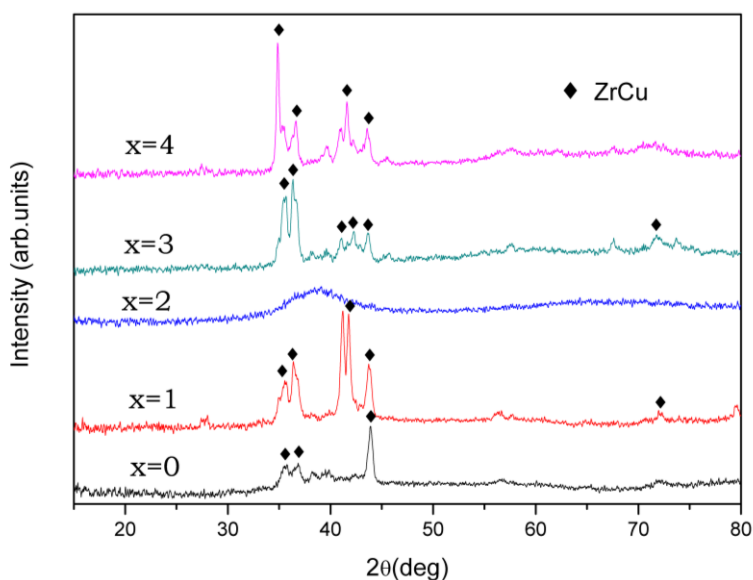


**Figure 1.** XRD patterns of  $\text{Cu}_{50}\text{Zr}_{50-x}\text{Y}_x$  ( $x=0, 1, 2, 3, 4$ ) rod samples

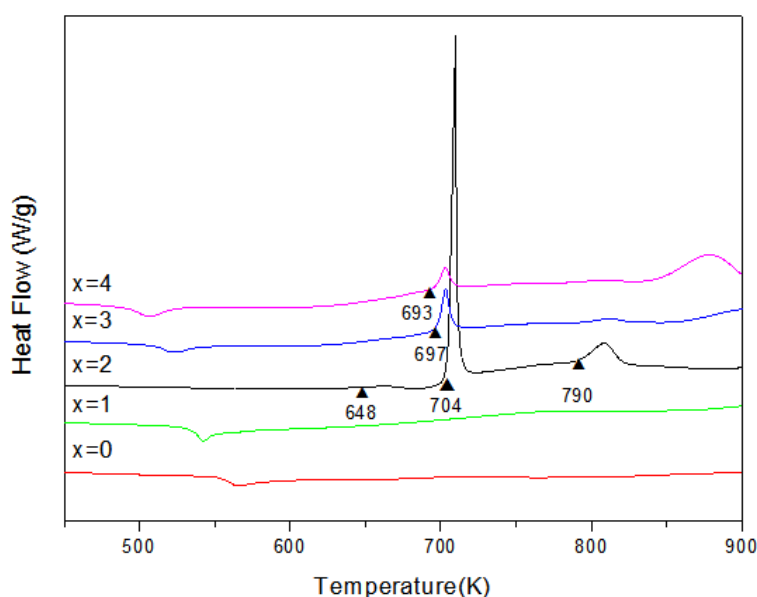
#### 3.2 Glass forming ability

Fig. 2 shows the DSC curves of  $\text{Cu}_{50}\text{Zr}_{50-x}\text{Y}_x$  ( $x=0, 1, 2, 3, 4$ ) rod samples.  $\text{Cu}_{50}\text{Zr}_{50}$  and  $\text{Cu}_{50}\text{Zr}_{49}\text{Y}_1$  alloy only have an endothermic peak, and no exothermic peak can be found.  $\text{Cu}_{50}\text{Zr}_{48}\text{Y}_2$  alloy has a weak endothermic peak around 550K, indicating a glass transition occurred. A relatively wide supercooled liquid region can be found when further increasing the temperature. In addition, there are two exothermic peaks can be seen in the DSC curve of  $\text{Cu}_{50}\text{Zr}_{48}\text{Y}_2$  alloy, implying a crystallization process with two steps. Thermal parameters of  $\text{Cu}_{50}\text{Zr}_{48}\text{Y}_2$  alloy which obtained from the DCS curve are shown in Table 1. The glass transition temperature ( $T_g$ ) and the initial crystallization temperature ( $T_{x1}$ ) of  $\text{Cu}_{50}\text{Zr}_{48}\text{Y}_2$  alloy are 648 K and 704 K, respectively. Correspondingly, the supercooled liquid region ( $\Delta T_x$ ) is 56 K, a little smaller than that of  $\text{Cu}_{49.5}\text{Zr}_{49.5}\text{Nd}_1$  in our previous research [17]. Comparing with the other type of Cu-Zr based BMG alloys,  $\text{Cu}_{50}\text{Zr}_{48}\text{Y}_2$  has a relatively high glass forming ability. The addition of Y can effectively improve the glass forming ability of  $\text{Cu}_{50}\text{Zr}_{50}$  alloy. Y is easier to react with oxygen than Cu and Zr in

the molten state, the generated  $Y_2O_3$  can precipitate in the surface of molten alloy and decrease the adverse impact of oxygen on the smelting and suction casting process. Additionally, Y has a relatively larger atomic radius ( $\sim 0.18$  nm) than that of Cu ( $\sim 0.128$  nm) and Zr ( $\sim 0.16$  nm). The difference of atomic radius between elements can influence the atomic rearrangement and restrain the growth of crystalline. Moreover, the relatively large negative mixing enthalpy (Y-Cu and Zr-Cu) can increase the random combination of different atoms and inhibit the long range diffusion, finally promote the formation of amorphous structure.

**Table 1.** Thermal parameters of  $Cu_{50}Zr_{48}Y_2$  alloy obtained from the DSC curves

Composition	$T_g/K$	$T_{x1}/K$	$\Delta T_x/K$
$Cu_{50}Zr_{48}Y_2$	648	704	56



**Figure 2.** DSC curves of  $Cu_{50}Zr_{50-x}Y_x$  ( $x=0, 1, 2, 3, 4$ ) rod samples with a heating rate of 20 K/min

### 3.3 Mechanical property

Fig.3 presents the microhardness of  $Cu_{50}Zr_{50-x}Y_x$  ( $x=0, 1, 2, 3, 4$ ) alloys. It can be seen that the microhardness of alloys are enhanced and varied significantly with the Y content.  $Cu_{50}Zr_{50}$  alloy has a relatively low hardness of  $\sim 443$   $HV_{100}$ . Following with the increasing Y content, the microhardness of alloys increased gradually and reached the peak of  $\sim 1017$   $HV_{100}$  when the Y concentration is 2 at. %. This hardness value is in the same level comparing with that of  $Cu_{49.5}Zr_{49.5}Nd_1$  ( $\sim 1044$   $HV_{100}$ ). Based on the DSC and XRD results, the peak microhardness value could be attributed to the amorphous

structure of  $\text{Cu}_{50}\text{Zr}_{48}\text{Y}_2$ . Further addition of Y leads to a decrease of microhardness but still keep at the level of above  $\sim 750\text{HV}_{100}$ , which is still much higher than  $\text{Cu}_{50}\text{Zr}_{50}$  alloy.

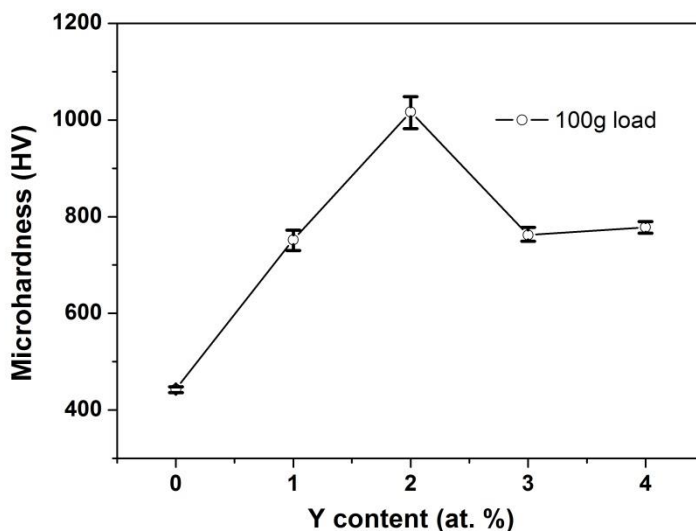


**Figure 3.** Microhardness of  $\text{Cu}_{50}\text{Zr}_{50-x}\text{Y}_x$  ( $x=0, 1, 2, 3, 4$ ) alloys

### 3.4 Corrosion resistance

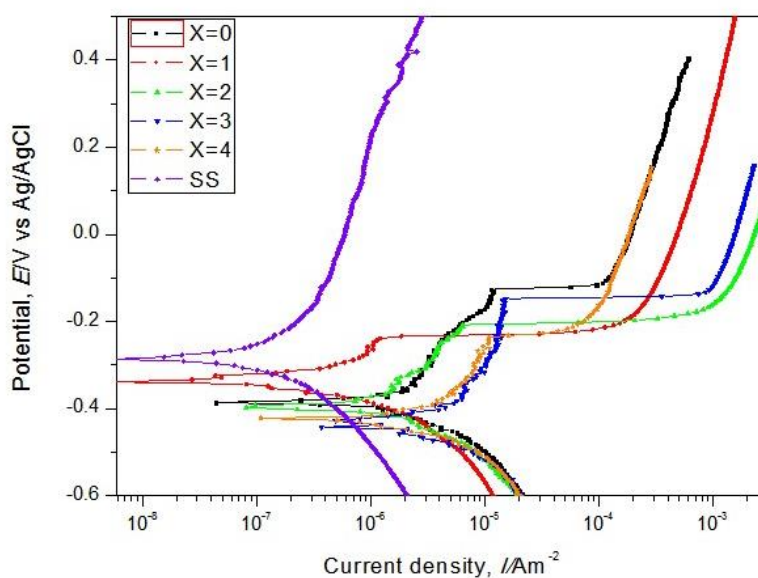


**Figure 4.** Potentiodynamic polarization curves of  $\text{Cu}_{50}\text{Zr}_{50-x}\text{Y}_x$  ( $x=0, 1, 2, 3, 4$ ) alloys in 0.1mol/L NaCl solution with a scanning rate of 0.33mV/s

Potentiodynamic polarization curves of  $\text{Cu}_{50}\text{Zr}_{50-x}\text{Y}_x$  ( $x=0, 1, 2, 3, 4$ ) alloys and stainless steel are shown in Fig.4. Table 2 shows the corrosion potential and corrosion current density which calculated from the potentiodynamic polarization curves. Stainless steel has the highest corrosion potential and lowest corrosion current density, presenting a better corrosion resistance than those of

Cu<sub>50</sub>Zr<sub>50-x</sub>Y<sub>x</sub> (x=0, 1, 2, 3, 4) alloys. Unlike stainless steel, all the curves of Cu<sub>50</sub>Zr<sub>50-x</sub>Y<sub>x</sub> (x=0, 1, 2, 3, 4) alloys have a clear passivation area, indicating a passive film was formed on their surface during the measurement process [19]. The passivation area of Cu<sub>50</sub>Zr<sub>50-x</sub>Y<sub>x</sub> (x=0, 1, 2, 3, 4) alloys grow wider after adding Y.

**Table 2.** E<sub>corr</sub> and I<sub>corr</sub> of Cu<sub>50</sub>Zr<sub>50-x</sub>Y<sub>x</sub> (x=0, 1, 2, 3, 4) alloys in 0.1mol/L NaCl solution with a scanning rate of 0.33mV/s

Sample	E <sub>corr</sub> (V vs. SCE)	I <sub>corr</sub> (A/cm <sup>2</sup> )
Stainless steel	-0.28	2.42×10 <sup>-7</sup>
Cu <sub>50</sub> Zr <sub>50</sub>	-0.39	7.67×10 <sup>-7</sup>
Cu <sub>50</sub> Zr <sub>49</sub> Y <sub>1</sub>	-0.33	3.55×10 <sup>-7</sup>
Cu <sub>50</sub> Zr <sub>48</sub> Y <sub>2</sub>	-0.40	1.07×10 <sup>-6</sup>
Cu <sub>50</sub> Zr <sub>47</sub> Y <sub>3</sub>	-0.44	2.38×10 <sup>-6</sup>
Cu <sub>50</sub> Zr <sub>46</sub> Y <sub>4</sub>	-0.42	1.69×10 <sup>-6</sup>

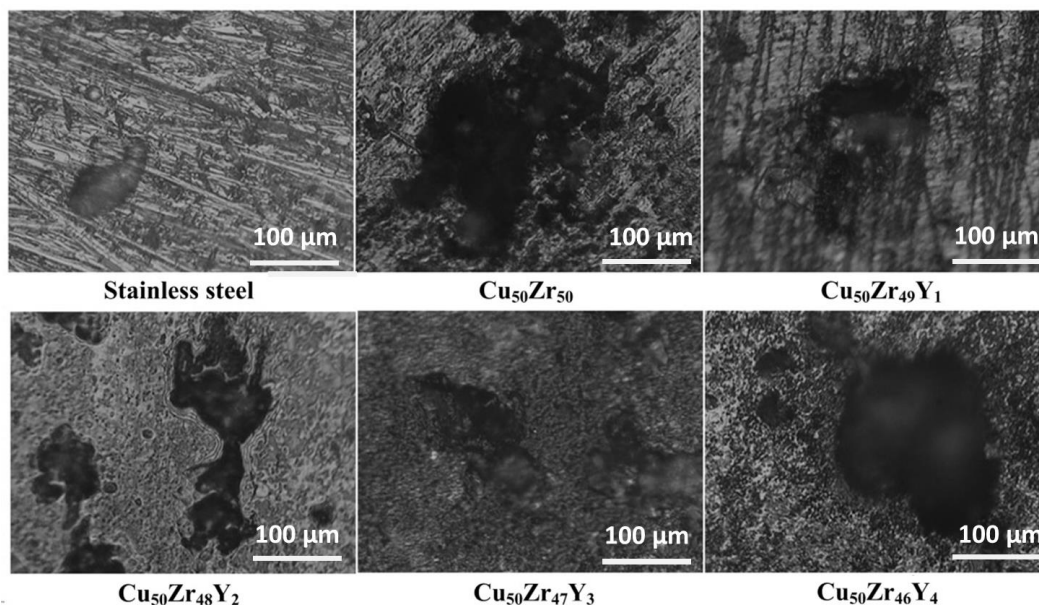


**Figure 5.** Metallography of stainless steel and Cu<sub>50</sub>Zr<sub>50-x</sub>Y<sub>x</sub> (x=0, 1, 2, 3, 4) alloys after corrosion test

Fig. 5 shows the surface morphology of stainless steel and Cu<sub>50</sub>Zr<sub>50-x</sub>Y<sub>x</sub> (x=0, 1, 2, 3, 4) alloys after testing. It can be seen that the stainless steel has a good corrosion resistance and only a small area was corroded. Correspondingly, a large pitting area can be found in Cu<sub>50</sub>Zr<sub>50</sub> alloy, indicating a more serious corrosion occurred. The passive films generated on their surface were penetrated during the measurement process. After adding Y, although the corrosion resistance of alloys were increased comparing with that of Cu<sub>50</sub>Zr<sub>50</sub> alloy, apparent pitting area still can be found in metallography pf

$\text{Cu}_{50}\text{Zr}_{50-x}\text{Y}_x$  ( $x=0, 1, 2, 3, 4$ ) alloys. CuY-type phase is feasible to preferential corrosion as convinced by Zhang et al. (2016) in the corrosion morphologies of CuZrY/Al, Ti, Hf series high-entropy alloys [20]. Additionally, according to the research conducted by Lu et al. (2008), the surface characteristics play an important role in influencing the corrosion resistance of the Cu-Zr glassy alloys [21]. Overall, the mechanism of how Y element alters the corrosion resistance of Cu-Zr glassy alloys is not very clear. Further research on improving corrosion resistance of Cu-Zr glassy alloys is being conducted.

#### 4. CONCLUSION

Different amounts of Y were added in order to increase the glass forming ability of Cu-Zr alloy. The microstructure, glass forming ability, mechanical property and corrosion resistance of  $\text{Cu}_{50}\text{Zr}_{50-x}\text{Y}_x$  ( $0 \leq x \leq 4\text{at.}\%$ ) alloys were systematically analyzed investigated.  $\text{Cu}_{50}\text{Zr}_{48}\text{Y}_2$  alloy presents an amorphous structure and has the best mechanical property comparing with the other alloys. The microhardness of  $\text{Cu}_{50}\text{Zr}_{48}\text{Y}_2$  alloy can reach  $\sim 1017$  HV compared to  $\sim 443$  HV of  $\text{Cu}_{50}\text{Zr}_{50}$  alloy. After adding Y, the corrosion resistance of alloys was increased comparing with that of  $\text{Cu}_{50}\text{Zr}_{50}$  alloy but still cannot compare with stainless steel. Further research on corrosion mechanism is being conducted in order to optimize the corrosion resistance of Cu-Zr-Y alloys.

#### ACKNOWLEDGEMENT

This work is supported by the financial support from the National Natural Science Foundation of China (No. 51202146 and 51601073), Natural Science Foundation of Shanghai (No. 17ZR1419700) and Jiangsu Distinguished Professor Project (No. 1064901601).

#### References

1. P. Tsai and KM. Flores, *Acta. Mater.*, 120 (2016) 426-434.
2. S. Y. Ding, Y. H. Liu, Y. L. Li, Z. Liu, S. Sohn, F. J. Walker and J. Schroers, *Nat. Mater.*, 13 (2014) 1-7.
3. A. Inoue and A. Takeuchi, *Acta. Mater.*, 59 (2011) 2243-2267.
4. C. A. Schuh, Todd C. Hufnagel and U. Ramamurty, *Acta. Mater.*, 55 (2007) 4067-4109.
5. W.H. Wang, C. Dong and C.H. Shek, *Mat. Sci. Eng. R.*, 44 (2004) 45-89.
6. D. V. Louzguine-Luzgin, G. Xie, Q. Zhang, C. Suryanarayana and A. Inoue, *Metall. Mater. Trans. A.*, 90 (2016) 145-150.
7. J. L. Wu, Y. Pan, X. Z. Li and X. F. Wang, *Mater. Design.*, 61 (2014) 199-202.
8. Z. L. Ning, W. Z. Liang, M. X. Zhang, Z. Z. Li, H. C. Sun, A. L. Liu and J. F. Sun, *Mater. Design.*, 90 (2016) 145-150.
9. W. Zhang, Q. Zhang and A. Inoue, *Adv. Eng. Mater.*, 10 (2008) 1034-1038.
10. B. F. Lu, L. T. Kong, Z. Jiang, Y. Y. Huang, J. F. Li and Y. H. Zhou, *J. Mater. Sci.*, 49 (2014) 496-503.
11. Y. Pan, Y. Q. Zeng, L. J. Jing, L. Zhang and J. H. Pi, *Mater. Design.*, 55 (2014) 773-777.
12. D. Q. Zhou, Y. Wu, H. Wang, X. D. Hui, X. J. Liu and Z. P. Lu, *Comp. Mater. Sci.*, 79 (2013) 187-192.
13. Y. Wu, H. Wang, H. H. Wu, Z. Y. Zhang, X. D. Hui, G. L. Chen, D. Ma, X. L. Wang and Z. P. Lu, *Acta. Mater.*, 59 (2011) 2928-2936.

14. A. Inoue, W. Zhang, T. Zhang and K. Kurosaka, *Acta. Mater.*, 49 (2001) 2645-2652.
15. D. Wang, Y. Li, B. B. Sun, M. L. Sui, K. Lu and E. Ma, *Appl. Phys. Lett.*, 84 (2004) 4029-4031.
16. B. Li, J. S. Li, X. H. Fan and J. Chen, *Rare. Metal. Mat. Eng.*, 43 (2014) 1558-1561.
17. X. Li, F. Lv, Y. X. Geng, F. Qi, Y. J. Xu, F. Liu and Y. X. Wang, *Int. J. Electrochem. Sci.*, 12 (2017) 726-732.
18. A. Inoue, W. Zhang and T. Zhang, *J. Non-Cryst Solids.*, 304 (2002) 200-209.
19. A. Y. Chen, S. S. Shi, H. L. Tian, H. H. Ruan, X. Li, D. Pan and J. Lu, *Mat. Sci. Eng. A.*, 595 (2014) 34-42.
20. Z. T. Zhang, E. Axinte, W. J. Ge, C. Y. Shang and Y. Wang, *Mater. Design.*, 108 (2016) 106-113.
21. H. B. Lu, L. C. Zhang, A. Gebert and L. Schultz, *J. Alloy. Compd.*, 462 (2008) 60-67.

© 2017 The Authors. Published by ESG ([www.electrochemsci.org](http://www.electrochemsci.org)). This article is an open access article distributed under the terms and conditions of the Creative Commons Attribution license (<http://creativecommons.org/licenses/by/4.0/>).